



Magnetic anisotropy and relaxation behavior of six-coordinate tris(pivalato)-Co(II) and -Ni(II) complexes

Journal:	<i>Dalton Transactions</i>
Manuscript ID	DT-ART-04-2018-001554.R1
Article Type:	Paper
Date Submitted by the Author:	23-Jun-2018
Complete List of Authors:	<p>Chen, Shu-Yang; Coordination Chemistry Institute, State Key Laboratory of Coordination Chemistry Cui, Hui-Hui; Coordination Chemistry Institute, State Key Laboratory of Coordination Chemistry Zhang, Yi-Quan; School of Physical Science and Technology, Physical department Wang, Zhenxing; Huazhong University of Science and Technology, Wuhan National High Magnetic Field Center; Ouyang, Zhongwen; National High Magnetic Field Center, Huazhong University of Science and Technology, Chen, Lei; Jiangsu University of Science and Technology, School of Environmental and Chemical Engineering Chen, Xue-tai; Coordination Chemistry Institute, State Key Laboratory of Coordination Chemistry; Yan, Hong; Nanjing University, State Key Laboratory of Coordination Chemistry Xue, Ziling; University of Tennessee, Department of Chemistry</p>

Magnetic anisotropy and relaxation behavior of six-coordinate tris(pivalato)-Co(II) and -Ni(II) complexes

Shu-Yang Chen,^a Hui-Hui Cui,^a Yi-Quan Zhang,^{b*} Zhenxing Wang,^{c*} Zhong-Wen Ouyang,^c Lei Chen,^d Xue-Tai Chen,^{a*} Hong Yan,^a Zi-Ling Xue^e

Abstract: Experimental and theoretical studies of magnetic anisotropy and relaxation behavior of six-coordinate tris(pivalato)-Co(II) and -Ni(II) complexes (NBu₄)[M(piv)₃] (piv = pivalate, M = Co, **1**; M = Ni, **2**), with coordination configuration at the intermediate between octahedron and trigonal prism, are reported. Direct current magnetic data and high-frequency and -field EPR spectra (HFEP) of **1** have been modeled by a general Hamiltonian considering the first-order orbital angular momentum, while the spin Hamiltonian was used to interpret the data of **2**. Both **1** and **2** show easy-axis magnetic anisotropies, which are further supported by *ab initio* calculations. Alternating current (ac) magnetic susceptibilities reveal slow magnetic relaxation at an applied dc field of 0.1 T in **1**, which is characteristic of a field-induced single-ion magnet (SIM), but **2** does not exhibit single-ion magnet

^aState Key Laboratory of Coordination Chemistry, School of Chemistry and Chemical Engineering, Nanjing University, Nanjing 210023, China. E-mail: xtchen@nju.edu.cn.

^bJiangsu Key Laboratory for NSLSCS, School of Physical Science and Technology, Nanjing Normal University, Nanjing 210023, China. Email: zhangyiquan@njnu.edu.cn

^cWuhan National High Magnetic Field Center & School of Physics, Huazhong University of Science and Technology, Wuhan 430074, China. Email: zxwang@hust.edu.cn

^dSchool of Environmental and Chemical Engineering, Jiangsu University of Science and Technology, Zhenjiang 212003, China.

^eDepartment of Chemistry, University of Tennessee, Knoxville, Tennessee 37996, USA.

†Electronic supplementary information (ESI) available: XRD patterns, calculations results and magnetic data.

property at 1.8 K. Detailed analyses of relaxation times show dominant contribution of a Raman process for spin relaxation in **1**.

Introduction

Single-molecule magnets (SMMs) are molecular species retaining the magnetization at low temperature after removing the external magnetic field due to the existence of energy barrier, which prevents the reversal of magnetic moment. Such molecular nanomagnets have showed potential applications in quantum computation, high density information storage, and molecular spintronics.¹ Initially many efforts were devoted to polynuclear 3d-based SMMs.² More recently, SMM behaviors have also been demonstrated in metal complexes containing single paramagnetic lanthanide,³ actinide,⁴ or transition metal ion,⁵ which are termed as single-ion magnets (SIMs). Since the first Fe(II)-SIM complex was reported by Long et al. in 2010,⁶ slow magnetic relaxation have been revealed in numerous d-ion complexes containing V(IV),⁷ Mn(III, IV),⁸ Fe(I, II, III)^{6,9} Co(I, II),¹⁰⁻¹² Ni(I, II),¹³ Cu(II)¹⁴, Cr(II),¹⁵ and Re(IV).¹⁶ Co(II)-SIMs constitute the largest family because of their non-integer ground-state spin and the large magnetic anisotropy.

Magnetic anisotropy is the most important origin for slow magnetic relaxation. The advantage of SIMs is that magnetic anisotropy can be easily fine-tuned by the interplay between ligand field splitting and spin-orbit interaction. For the majority of d-ion complexes,⁶⁻¹⁶ the first-order orbital momentum is usually quenched by ligand field. Thus, magnetic anisotropy arises from the coupling between a non-degenerate

electronic ground state and the orbitally degenerate excited state. Since such spin-orbital coupling is usually weak, the resulting magnetic anisotropy is mostly small, which can be modeled as zero-field splitting using axial and rhombic parameters D and E , respectively. However, in some cases where orbital momentum is unquenched or only partially quenched as in six-coordinate Co(II) complexes, the first-order spin-orbital coupling occurs and contributes to large magnetic anisotropy. In these cases, magnetic anisotropy cannot be modeled by the spin-only Hamiltonian with the D and E parameters. The mostly employed technique to probe magnetic anisotropy is the magnetometry. However, in the absence of the confirmative data from other physical techniques and theoretical calculations, the reliability of the results, especially the sign of the magnetic anisotropy derived, may be questioned. Thus, a combination analysis of various techniques (e.g. magnetometry and HFEPR) and theoretical calculation is usually required.

The coordination configurations of the reported Co(II)-SIMs are various along with the coordination number from two to eight.¹⁰⁻¹² Since the first example of six-coordinate field-induced Co(II) SIM was reported,^{11a} many Co(II) complexes with octahedral¹¹ or trigonal prismatic geometries,¹² which exhibit slow magnetic relaxation, have been reported. Most of six-coordinate Co(II)-complexes exhibit easy-plane magnetic anisotropy^{5,11a-11f} while only few examples with easy-axis anisotropy are known.^{11g-11n,12} Compared with these distorted octahedral geometry,¹¹ a trigonal prism is a better geometry to give large easy-axis magnetic anisotropy, which results in zero-field SIMs with a high energy barrier.^{12a-12e} For example, Gao et al.

have reported a series of mononuclear, six-oxygen-coordinated Co(II) complexes with distorted trigonal prismatic geometry and energy barriers in the range of 26.6–102.8 cm^{-1} .^{12a,12b} Winpenny et al. have also revealed a Co(II) cage complex with a trigonal prismatic configuration constructed by six nitrogen atoms, showing SIM behavior with an energy barrier of 152 cm^{-1} ,^{12c} which is relatively high among d-ion based SIMs. It is noted that the reported Co(II) complexes showing zero-field slow magnetic relaxation possess trigonal prismatic geometry with a twist angle smaller than 23.5°.^{11n,12}

Magnetic anisotropy of the Ni(II) complexes have been studied to a lesser extent compared to Co(II) complexes.¹⁷⁻¹⁹ HF-EPR has been successfully used to probe magnetic anisotropy of Ni(II) complexes of various coordination environments and geometries.¹⁸⁻¹⁹ However, the examples of Ni(II)-SIMs are rare, which include two octahedral Ni(II) complexes^{13b,13c} and one trigonal bipyramidal Ni(II) complex.^{13d}

With the aim to provide more experimental data on magnetic anisotropy dependent on coordination geometry, we have investigated direct current (dc) and alternating current (ac) magnetic properties of two mononuclear Co(II) and Ni(II) complexes $(\text{NBu}_4)[\text{M}(\text{piv})_3]$ (piv = pivalate, M = Co, **1**; M = Ni, **2**) with a coordination configuration at the mid-point between octahedron and trigonal prism. The dc magnetic data and high-frequency and -field EPR spectra show their easy-axis magnetic anisotropies, which have been supported by theoretical calculations at the XMS-CASPT2 level. Alternating current magnetic susceptibility data show that **1** is a field-induced single-ion magnet, while **2** does not exhibit the SIM behavior.

Furthermore, theoretical calculations have been performed to reveal the magnetostructural correlations between magnetic anisotropy and structural distortion.

Experimental section

General information

Complexes **1** and **2** were prepared according to the reported procedures.²⁰ Their identities were confirmed by elemental analyses (CHN) performed on an Elementar Vario ELIII elemental analyzer and infrared spectra measured on a Tensor 27 FT-IR spectrometer using KBr pellets in the range of 400-4000 cm^{-1} . The polycrystalline samples of **1** and **2** for magnetic and HFEPR studies were characterized by powder X-ray diffraction on a Bruker D8 ADVANCE X-ray powder diffractometer in the 2θ range of 5-50° at room temperature (Figs. S1-S2, ESI). HFEPR experiments were performed using a spectrometer constructed at National High Magnetic Field Laboratory, USA.²¹

Magnetic measurements

Magnetic measurements were performed on polycrystalline samples of **1** and **2** restrained in a frozen eicosane matrix using a Quantum Design SQUID VSM magnetometer. Direct current (dc) magnetic data were recorded at fields up to 7 T in the range of 2.0-300 K. Alternating current (ac) susceptibilities were measured using an oscillating ac field of 0.2 mT and ac frequencies ranging from 1 to 1000 Hz. Dc magnetic susceptibilities were corrected for diamagnetism using Pascal constants and a sample holder correction.

Results and discussion

Structural features

Crystal structures of **1** and **2** have already been reported.²⁰ Their main structural aspects related to magnetic properties are emphasized here. Their important crystal data and bond parameters are summarized in Table S1. The structures of **1** and **2** are presented in Figure 1. They are isostructural with the central metal ion displaying a six-coordinate geometry, in which three pivalate anions act as bidentate ligands with acute bite angle 61.86(8), 62.18(8), 62.00(8)° for **1** and 60.68(1), 61.48(1), 62.54(2)° for **2**. The M-O distances are in the range of 2.105(2)–2.147(2) Å in **1** and 2.045(4)–2.108(4) Å in **2**. The six coordinated oxygen atoms can be viewed as in the parallel upper and lower planes with a dihedral angle is 2.44° (**1**) and 1.79° (**2**). The twist angle φ , defined as the rotation angle of one coordination triangle away from the eclipsed configuration to the other, is 60° for an ideal octahedron and 0° for an ideal trigonal prism, respectively (Figure 2). The value of φ is 28.71° in **1** and 28.08° for **2**, respectively, which was calculated as the average of the six torsional angles obtained by connecting skewed O atoms from different triangles via the centroids of the two triangles. Therefore the coordination geometry in both complexes can be regarded as being at the mid-point of the octahedron and trigonal prism. In order to further evaluate the degree of the structural distortion, a continuous shape measurement analyses were performed using the SHAPE program.²² The calculated value provides an estimate of the distortion degree from the possible ideal structure, and the zero value corresponds to the ideal polyhedron. The obtained values relative to the ideal

octahedron and trigonal prism are 7.06, 9.34 for **1** and 6.56, 11.09 for **2**, respectively.

The two values are rather large, suggesting the great deviations of **1** and **2** from the two ideal configurations, consistent with their intermediate coordination configuration between octahedron and trigonal prism. The metal ions are well-separated for the shortest intermolecular Co---Co distances of 7.46 Å (**1**) and 7.50 Å (**2**), thus precluding any prominent intermolecular magnetic interactions.

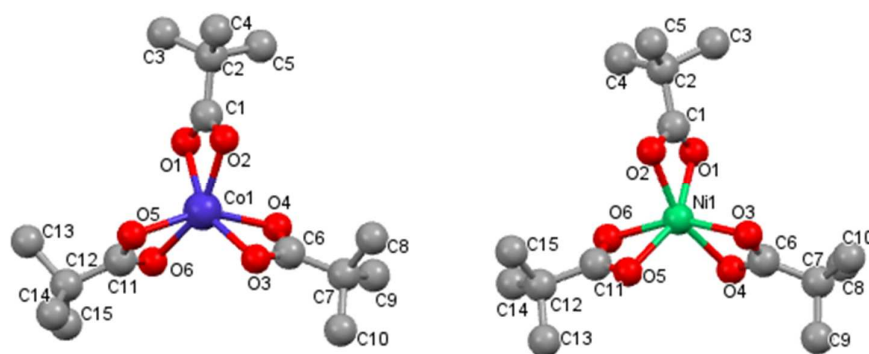


Figure 1 Structures of the anions in **1** (left) and **2** (right)

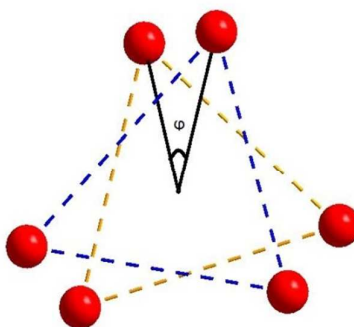


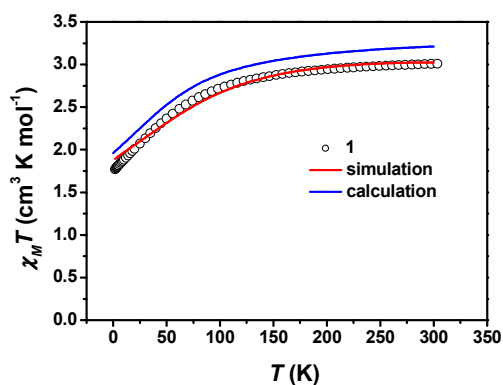
Figure 2 Twist angle ϕ of coordination polyhedron with respect to ideal trigonal prism.

Magnetic anisotropy of (NBu₄)[Co(piv)₃] (**1**)

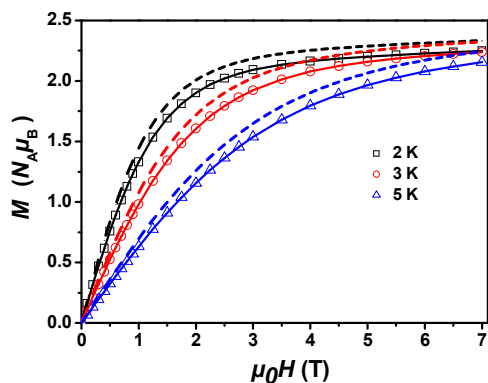
Magnetic anisotropy of **1** has been studied by dc magnetic measurements, HFEPR and theoretical calculations. Variable-temperature magnetic susceptibilities were measured for the polycrystalline sample of **1**. The resulting $\chi_M T$ vs T plot shown in Figure 3 is typical for a mononuclear Co(II) system with an orbital contribution to the magnetic moment. The $\chi_M T$ product is $3.00 \text{ cm}^3 \text{ K mol}^{-1}$ at 300 K, larger than the expected value of $1.875 \text{ cm}^3 \text{ K mol}^{-1}$ for one isolated high spin Co(II) ion center ($S = 3/2$, $g = 2.0$), indicative of the strong orbital contribution.¹⁰⁻¹² Upon cooling from 300 K, the $\chi_M T$ value decreases gradually to the minimum value of $1.77 \text{ cm}^3 \text{ K mol}^{-1}$ at 2.0 K. As in other six-coordinate Co(II) complexes,¹¹⁻¹² such downturn indicates the presence of the strong orbital contribution, rather than the intermolecular interactions due to the long intermolecular distance between the Co(II) ions. The field-dependent magnetizations of **1** were measured from 1 to 7 T dc field at 2.0, 3.0, and 5.0 K (Figure 3b). With the increase of the magnetic field, the magnetization continuously increases and reaches $2.25 N_A \mu_B$ at 7 T and 2.0 K, smaller than the expected value of $3.0 N_A \mu_B$ ($g = 2.0$). The high-field non-saturation also suggests the presence of significant magnetic anisotropy.

In the six-coordinate Co(II) system such as **1**, where the unquenched orbital moment contribute strongly to the magnetic moment,²³ the fitting of the magnetic data could not define the sign of the magnetic anisotropy. As pointed out by Palli^{11f,11g} and Chilton,¹¹ⁱ a joint analysis of magnetic data with other spectroscopic data such as EPR should be performed. Thus, HFEPR spectra were measured for the polycrystalline sample of **1** at 10 K with different frequencies in the range of 50.8-428.5 GHz (Figure

4a). All the spectra present three features, consistent with the rhombic anisotropy. A 2D resonating field versus frequency map containing three linear branches was derived from the observed features (Figure 4b), indicating that these spectra can be interpreted in terms of an effective $S_{eff} = 1/2$ state and effective g values.^{11h,11i,11k} The 2D map was fit²⁴ to give the effective g values: $g_{x,eff} = 2.43$, $g_{y,eff} = 2.84$ and $g_{z,eff} = 6.77$. This pattern is consistent with easy-axis magnetic anisotropy of **1** with significant rhombic component.



(a)



(b)

Figure 3 (a) Variable-temperature dc susceptibility data of **1** under an applied dc field

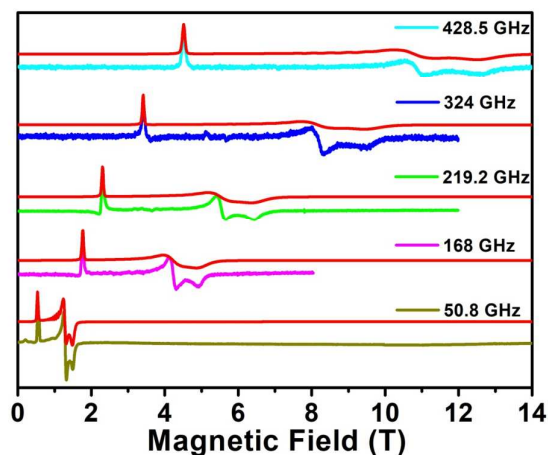
of 0.1 T. Red solid line represents the simulation using general Hamiltonian by the *PHI* program²⁵ and the blue one is the theoretical curve calculated by *MOLCAS* 8.2 program package;²⁷ (b) Field dependent magnetizations for **1**. Solid lines are the simulations using general Hamiltonian by the *PHI* program²⁵ while the dashed lines are the theoretical curves calculated by *MOLCAS* 8.2 program package.²⁷

The commonly used zero-field splitting parameters D and E cannot be used to present the single-ion magnetic anisotropy in the six-coordinate Co(II) complexes with easy-axis magnetic anisotropy.^{11f,11g,11i,23} The most trustworthy treatment of the dc magnetic data is the general Hamiltonian shown in equation 1, which takes into account the treatment of the first-order orbital angular momentum of Co(II).

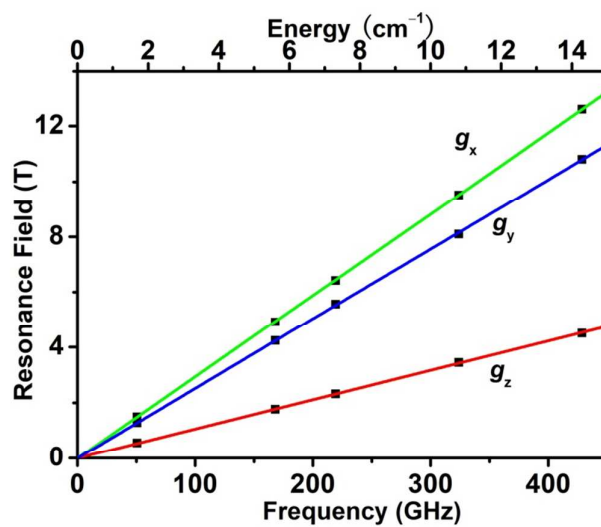
$$\hat{H} = \sigma\lambda\hat{L}\cdot\hat{S} + \sigma^2(B_2^0(3\hat{L}_z^2 - \hat{L}^2) + \frac{B_2^2}{2}(\hat{L}_+^2 + \hat{L}_-^2)) + \mu_B(\sigma\hat{L} + 2\hat{S})B \quad (1)$$

where σ is the combined orbital reduction factor defined as $\sigma = -A\cdot\kappa$. The A parameter is required when using the T \equiv P equivalence for orbital triplet terms^{23a,25} and takes the value of 1.0 when representing a T₂ term and 3/2 when representing a T₁ term. The κ parameter considers the reduction of the orbital momentum caused by the delocalization of the unpaired electrons. λ is the spin-orbit coupling parameter, B_2^0 and B_2^2 are crystal field parameters (CFPs).^{11i,23,25} To avoid the overparameterisation, we fix the spin-orbit coupling parameter for Co(II) ion to $\lambda = -170 \text{ cm}^{-1}$ and treat both HFEP and magnetic data with three parameters σ , B_2^0 and B_2^2 . In order to reproduce the observed of $g_{x,eff} < g_{y,eff} < g_{z,eff}$ in HFEP spectra, B_2^0 should be negative. We found the excellent agreement with the HFEP g_{eff} values using $\sigma = 1.33(0)$, $B_2^0 = -134.4$

cm^{-1} and $B_2^2 = 37.5 \text{ cm}^{-1}$ (Figure 4a). These parameters also lead to the simulated magnetic curves, which agree well to the experimental magnetic data (Figure 3).



(a)



(b)

Figure 4 (a) HFEPR spectra of **1** recorded at 10 K with various microwave frequencies. The red lines represent the simulations with the full Hamiltonian using the Hamiltonian parameters in the text by using PHI ,²⁵ (b) 2D field/frequency map of

HFEPR transitions in **1**. The squares are the experimental points while green, blue, and red curves are generated by the fitting by *SPIN*^{24a} with the magnetic field *B* parallel to the *x*, *y*, and *z* axis of the ZFS tensor, respectively.

In order to get further insight into the electronic structure of **1**, theoretical calculations were carried out at *XMS-CASPT2*²⁶ level using the *MOLCAS* 8.2 program package.²⁷ Calculation details are given in ESI. The energies of the spin-free states and spin-orbit states were calculated for **1**, which are listed in Tables S2-S4. The energy difference (447.1 cm⁻¹) between the lowest two spin-free states (Table S2) is larger than that between the lowest two spin-orbit states (167.6 cm⁻¹, Table S4). However, the spin-orbit ground state is composed of the lowest three spin-free states, not just formed from the ground one (Table S3). These suggest that there is very strong first-order spin-orbital coupling in **1** and zero-field splitting parameters *D* and *E* cannot be used to depict its magnetic anisotropy. The calculated *S* = 1/2 effective *g*-values of the ground state Kramers doublet of the Co^{II} of **1**, *g*_x = 2.194, *g*_y = 3.345, and *g*_z = 6.835, are well consistent with those from EPR spectra. The calculated orientations of the *g*_x, *g*_y, *g*_z (hard axis) of the ground doublet on the Co^{II} ion were shown in Figure S4. The direction of the easy axis is approximately along the *C*₃-axis of **1**. Furthermore, magnetic susceptibilities and magnetizations of **1** were also calculated as shown in Figure 3, which are comparable to the experimental curves.

These results support the negative sign of magnetic anisotropy in **1**. The same negative anisotropy has been reported for the six-coordinated Co(II)-complexes with

trigonal prismatic geometry.¹²

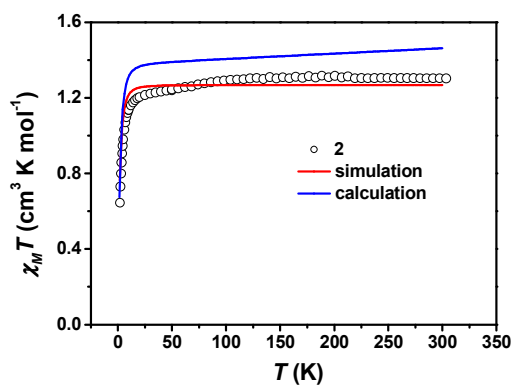
Magnetic anisotropy of (NBu₄)[Ni(piv)₃] (**2**)

Direct current magnetic data were measured for polycrystalline sample of **2** (Figure 5). Its $\chi_M T$ product is 1.30 cm³ K mol⁻¹ at 300 K, which is larger than the theoretical $\chi_M T$ value (1.16 cm³ K mol⁻¹, $g = 2.15$) for six-coordinate Ni(II) ion with largely quenched orbital moment. $\chi_M T$ value remains roughly constant in the range of 300-20 K, then decreases abruptly to 0.64 cm³ K mol⁻¹ at 2.0 K. The field-dependent magnetizations of **2** were measured from 1 to 7 T at 2.0, 3.0, and 5.0 K (Figure 5b). The magnetization continuously increases with the magnetic field and reaches 2.03 $N_A \mu_B$ at 7 T at 2.0 K, close to the expected value of 2.0 $N_A \mu_B$ ($S = 1$, $g = 2.0$).

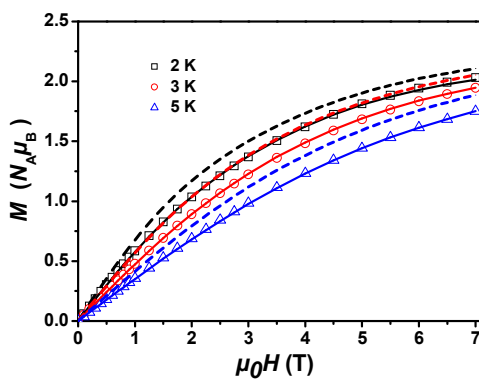
For six-coordinate Ni(II) complex, the effective spin-Hamiltonian with the axial and rhombic zero-field splitting (ZFS) parameters as showed in equation 2 can be used to present the magnetic anisotropy,^{13,17-19}

$$\hat{H} = D(\hat{S}_z^2 - S(S+1)/3) + E(\hat{S}_x^2 - \hat{S}_y^2) + \mu_B g \hat{S} B \quad (2)$$

Here, μ_B denotes the Bohr magneton and D , E , S and B represent the axial and rhombic ZFS parameters, the spin, and the magnetic field vector, respectively. The $\chi_M T$ data and magnetization curves were fit simultaneously using the *PHI* program.²⁵ The fitting gives a set of parameters $D = -7.86(4)$ cm⁻¹, $E = 0.76(2)$ cm⁻¹, $g_x = g_y = 2.440(3)$ and $g_z = 1.918(4)$.



(a)



(b)

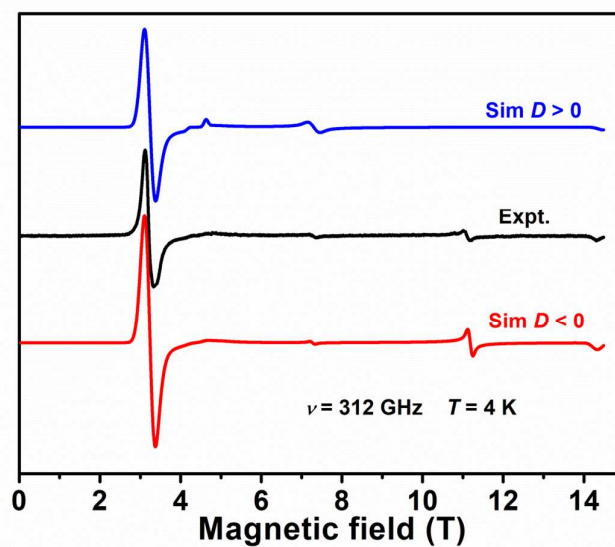
Figure 5 (a) Variable-temperature dc susceptibility data of **2** under an applied dc field of 0.1 T. Red solid line represents the simulation using general Hamiltonian by the *PHI* program²⁵ and the blue one is the theoretical curve calculated by *MOLCAS* 8.2 program package;²⁷ (b) Field dependent magnetizations for **2**. Solid lines are the simulations using general Hamiltonian by the *PHI* program²⁵ while the dashed lines are the theoretical curves calculated by *MOLCAS* 8.2 program package.²⁷

The easy-axial type of magnetic anisotropy of Ni(II) in **2** was further studied by

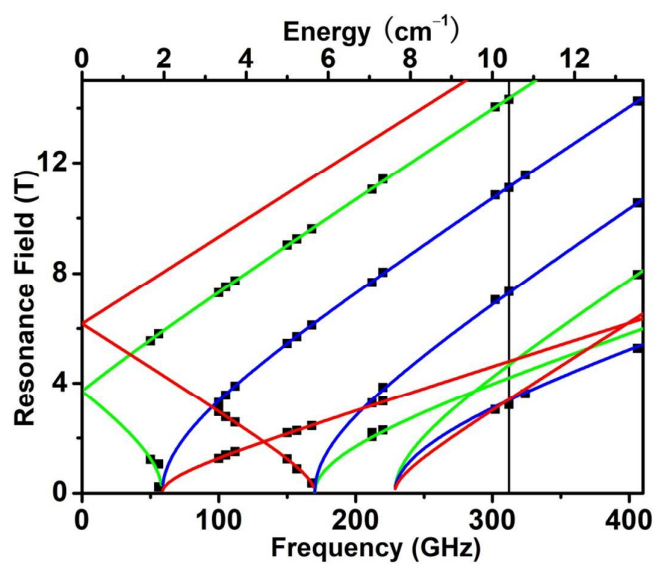
tunable-frequency HFEP spectra^{18a} with frequency range from 56 to 406 GHz up to 14.5 T. The spectra are typical of an $S = 1$ spin state. An EPR spectrum recorded at 312.0 GHz and 4 K is shown in Figure 6a. The main feature of the spectra is a very intense transition at low field, denoted as B_{min} , and the three others being much weaker. The former is due to the off-axis turning point of the forbidden ($\Delta Ms = \pm 2$) transition, which is usually the highest peak in the triplet powder spectrum.²⁸ More information can be derived from the 2D resonating field versus frequency map extracted from the turning points of the series of EPR spectra (Figure 6b). All the experimental points can be simultaneously fit^{24a} by spin Hamiltonian to give the optimal parameters: $|D| = 6.65(6) \text{ cm}^{-1}$, $E = 0.98(2) \text{ cm}^{-1}$, $g_x = 2.23(2)$, $g_y = 2.24(2)$, and $g_z = 2.28(5)$. In order to reveal the sign of D value, the EPR spectrum recorded at 312.0 GHz and 4 K was also simulated using the above Hamiltonian parameters. The blue and red traces are the simulated spectra using the positive and negative D values, respectively, which prove a negative D value for **2**. These parameters are also within the zero-field splitting parameters reported for the six-coordinate Ni(II) complexes determined by HFEP techniques.¹⁹

The Hamiltonian parameters determined by HFEP cannot provide a good agreement to the experimental magnetic data especially the magnetization data (Figure S5). If the g values are fixed as those determined by HFEP, the fitting of magnetic data gave D and E values being $-7.78(22)$ and $1.38(6) \text{ cm}^{-1}$ (Figure S6). Such inconsistency between the Hamiltonian parameters from HFEP and magnetic data is not unusual.²⁹ It is well known that the fitting of magnetic data would not give

the reliable Hamiltonian parameters, which could be due to the occurrence of impurities, the possible weak intermolecular interactions, the orientation of the microcrystals under the magnetic field and other undefined structures.^{19f-19h}



(a)



(b)

Figure 6 (a) HF-EPR spectrum of **2** with its simulations at 312.0 GHz and 4 K (blue trace: positive D ; green trace: negative D); (b) Resonance field vs microwave frequency of EPR transitions in **2**. The squares are the experimental points while green, blue, and red curves are generated by the fittings^{24a} using the spin Hamiltonian parameters indicated in the text with the magnetic field B parallel to the x , y , and z axis of the ZFS tensor, respectively. The vertical line represents the frequency (312.0 GHz) at which the spectra shown in Figure 6a were taken.

The zero-field splitting parameters of **2** were calculated at the XMS-CASPT2 level²⁶ using the *MOLCAS* 8.2 program package.²⁷ The calculated D , E (cm^{-1}) and g tensor (x , y , z) of **2** are listed in Table S5, where the calculated D (-7.1 cm^{-1}) and E (1.2 cm^{-1}) values agree well with those determined by HFEPR spectra ($D = -6.67(6)$, $E = 0.96(2) \text{ cm}^{-1}$). The orientation of the easy axis of the ground doublet on Ni^{II} ion is also approximately along the C_3 -axis in **2** (Figure S4). The calculated magnetic susceptibilities and magnetizations of **2** shown in Figure 5 are comparable to the experimental curves. These results furthermore support the easy-axis magnetic anisotropy of **2**.

Magnetic relaxation by ac magnetic susceptibility studies

Alternating current susceptibility measurements were performed for **1** and **2** in order to study the low temperature dynamic magnetic behavior. No out-of-phase ac susceptibility (χ_M'') signal was observed for **1** under zero applied dc field at 1.8 K (Figure S7a), which is probably due to the occurrence of quantum tunneling of the

magnetization (QTM). The application of an external magnetic field could induce the frequency-dependent ac susceptibilities (Figure S7a), suggesting that the QTM phenomenon could be suppressed. For **1**, the maximum of χ_M'' appears at 0.04 T, which becomes the strongest with the increasing of the applied magnetic field up to 0.1 T. Therefore an optimum magnetic field of 0.1 T was used for temperature- and frequency-dependent ac susceptibility measurements in the temperature range of 1.8-6.0 K (Figures 7a and S8). A frequency-dependent signal was observed below 6 K as shown in the χ_M'' vs T plot (Figure S8), suggesting field-induced slow magnetic relaxation.

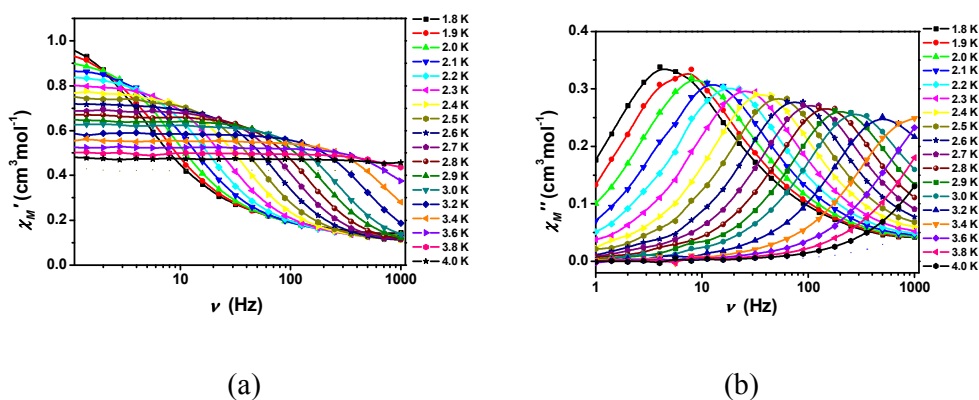


Figure 7 Frequency dependence of in-phase (χ_M') (a) and out-of-phase (χ_M'') (b) ac magnetic susceptibilities from 1.8 to 4.0 K under 0.1 T dc field for **1**. The solid lines are for eye guide.

In contrast with **1**, no significant χ_M'' signals were observed for **2** with the frequency of 1-1000 Hz at 1.8 K under an applied magnetic field in the range of 0-0.1 T (Figure S7b), suggesting that **2** does not exhibit the SIM property at 1.8 K.

The Cole–Cole plots were created from the alternating current data of **1** and fit using the generalized Debye model³⁰ based on equation 3 to extract the values and distribution of the relaxation times:

$$\chi_{ac}(\omega) = \chi_S + \frac{\chi_T - \chi_S}{1 + (i\omega\tau)^{(1-\alpha)}} \quad (3)$$

where χ_T and χ_S are the isothermal and the adiabatic susceptibility, respectively; ω is angular frequency; τ is relaxation time; α indicates deviation from a pure Debye model.³¹ As shown in Figure S9, the Cole-Cole plots of χ_M'' vs χ_M' between 1.8 and 3.4 K have semicircular profiles, indicative of a single relaxation process. The fitting parameters are summarized in Table S6. The parameter α is in the range of 0.05-0.25 and is found to increase with the decreasing of temperature, suggesting a small distribution of relaxation times.

The obtained values of relaxation time in the range 1.8 to 3.4 K were fit by the Arrhenius law $\tau = \tau_0 \exp(U_{\text{eff}}/kT)$ to give $U_{\text{eff}} = 20.7 \text{ cm}^{-1}$ ($\tau_0 = 2.69 \times 10^{-8} \text{ s}$) for **1** (Figure S10). This derivation of the effective energy barrier was based on the assumption that the dominant relaxation mechanism is the thermally activated Orbach process in the studied temperature range. In fact, the Orbach mechanism is not necessarily the dominant process, at least in the investigated temperature range. The obvious curvature in the Arrhenius plot of **1** implies that non-negligible Raman process could contribute to the relaxation rate. On this ground, a model including Orbach and Raman mechanisms was used to analyze the contribution to the relaxation rate in **1** by equation 4:³¹

$$\tau^{-1} = CT^n + \tau_0^{-1} \exp(-U_{\text{eff}}/kT) \quad (4)$$

Here, the two terms represent the contributions of the Raman and Orbach processes, respectively. The best fitting of the relaxation time vs temperature curves give the following parameters: $n = 5.7$, $C = 1.1 \text{ s}^{-1} \text{ K}^{-5.7}$, $\tau_0 = 1.2 \times 10^{-8} \text{ s}$, and $U_{eff} = 23.1 \text{ cm}^{-1}$. The fit reproduces the experimental data very well (Figure S11). The using of Orbach model implies that an excited state exists at an energy separation of 23.1 cm^{-1} above the ground state to provide the intermediate state for the relaxation process. But the first excited state is theoretically predicted to be 167.7 cm^{-1} higher than the ground state for **1**. Therefore the Orbach process is unlikely to be involved in magnetic relaxation in **1**. When the Orbach mechanism is neglected, the relaxation time data could be fit by a power law $\tau^{-1} = CT^n$ to give the resulting values $n = 8.3$ and $C = 0.19 \text{ s}^{-1} \text{ K}^{-8.3}$ (Figure 8). The obtained n value is very close to the expected $n = 9$ for Raman mechanism in Kramers ions, suggesting the dominant contribution of a Raman process for the spin relaxation in **1**.³¹

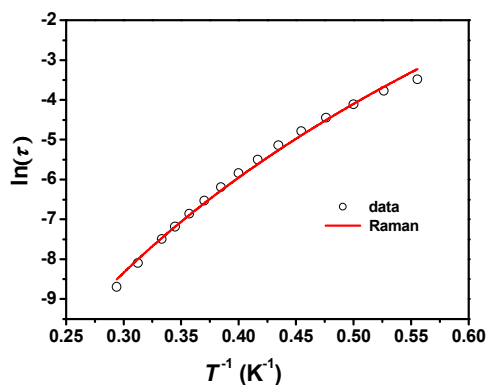


Figure 8 $\ln(\tau)$ vs T^{-1} plot of complex **1**.

Several reported Co(II) complexes showing zero-field slow magnetic relaxation possess distorted trigonal prismatic geometry with a twist angle smaller than 23.5° .^{11n,12} Complex **1** displaying slow magnetic relaxation under a magnetic field has a twist angle of 28.7° . Dunbar and Song et al. have reported field-induced slow magnetic relaxation in several Co(II) complexes with trigonal antiprismatic configuration with twist angles close to 60° .¹¹ⁱ⁻¹¹ⁿ To get further insight into magnetic anisotropy in tris(pivalato)-Co(II) and -Ni(II) complexes, we carried out further theoretical studies on a series of model complexes with twist angle φ from 0 to 60° by rotating the one O3 plane relative to the other. For each model complex of Co(II), the energy level and the \mathbf{g} tensor of the ground and first excited doublets of Co(II) ion were calculated using XMS-CASPT2²⁶ with *MOLCAS* 8.2.²⁷ The calculation results are summarized in Figure 9 and Table S7. When the twist angle φ is zero, corresponding to a trigonal prismatic geometry, g_x and g_y values are nearly zero and g_z is 9.572, which is of highly axial anisotropy. With the φ becomes larger, the g_x and g_y increase but g_z decreases, reaching a cross-over point at about 35° , where three g values are identical. Further increasing the φ angle, g_x and g_y become larger than g_z , showing the easy-plane anisotropy. These trend leads to an important conclusion that the Co(II) ion possess easy-axis magnetic anisotropy when a twist angle is smaller than 35° while positive anisotropy is found with a twisting angle larger than 35° . Similar crossover from easy-axis to easy-plane anisotropy has been predicted in a CoN_6 system.^{12e} Furthermore, the increasing of g_x and g_y with φ suggests the enhanced transversal anisotropy in Co(II). In **1** with a twist angle φ of 28.7° , the quantum

tunnelling of the magnetization (QTM) induced by a transversal magnetic field ($2\Delta_{\text{tun}} = \mu_B[g_x^2 H_x^2 + g_y^2 H_y^2]^{1/2}$) might be strong.³² Moreover, the discrepancy between g_x and g_y in **1** also promotes the QTM. Thus, no slow magnetic relaxation is observed in **1** under zero field. Accompanying with the above trend, the energy gap between the ground and the first excited state also varies with ϕ (Figure 10b). With the increasing of ϕ from zero, the energy gap decreases and reaches a minimum at 40° and then increases again. The minimum value corresponds to the cross-over point.

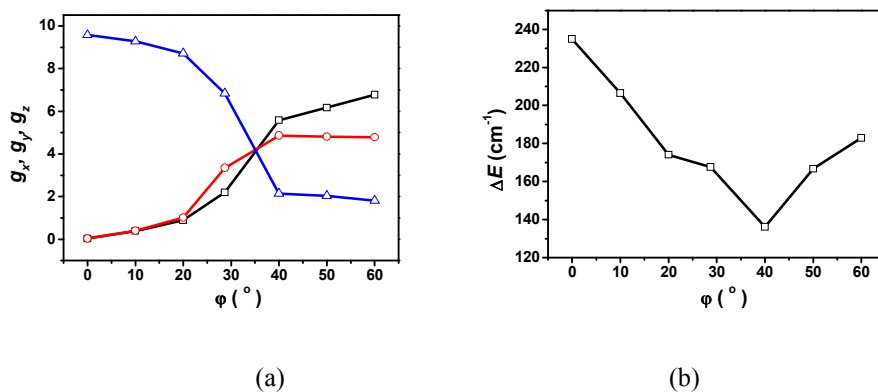


Figure 9 The correlation among twist angle ϕ ($^\circ$) and g_x (black), g_y (red), and g_z (blue) (a) and the energy gap (cm^{-1}) (b) in Co(II) complexes.

The g values and zero field splitting parameters D and E were calculated for a series of model complexes with different twist angles derived from **2**, which are summarized in Figure 10 and Table S8. With twist angle ϕ increasing from zero, Ni(II) complex exhibits easy-plane anisotropy and then easy-axis anisotropy through a crossover point at the twist angle of ca 25° . Our complex **2** is nearly at the cross-over point and has a small negative D value, which could be the reason why no slow

magnetic relaxation was observed for **2** even under a magnetic field. Comparison of the above calculated results of the model complexes based on **1** and **2**, we can conclude that at the two extremes of coordination configuration, i.e. trigonal prism geometry or trigonal antiprism, Co(II) and Ni(II) complexes would exhibit the opposite anisotropy. To have large and negative anisotropy, trigonal prism is better for Co(II) while trigonal antiprism is the choice for Ni(II).

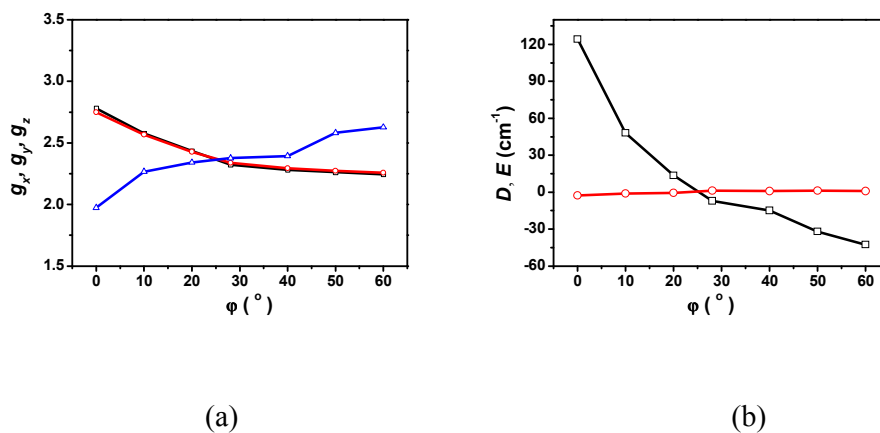


Figure 10 The correlation between twist angle ϕ ($^\circ$) and g_x (black), g_y (red), and g_z (blue) (a) and D (black) and E (red) (b) in Ni(II) complexes.

Conclusions

The static and dynamic magnetic studies have been performed on mononuclear, six-coordinated Co(II) and Ni(II) complexes $(\text{NBu}_4)[\text{M}(\text{piv})_3]$ (piv = pivalate, M = Co, **1**; M = Ni, **2**) with a configuration at the midpoint between the octahedron and trigonal prism. The joint studies employing magnetic measurements, HFEPR spectroscopy and theoretical calculations confirm the negative sign of magnetic

anisotropy in **1** and **2**. The ac magnetic susceptibility data show that **1** is a field-induced SIM, but **2** does not show magnetic relaxation at 1.8 K. While the six-coordinate Co(II) complexes with positive magnetic anisotropy are well studied, the examples of the complexes exhibiting field-induced SIM properties due to the negative magnetic anisotropy are relatively scarce. This work adds a new number of six-coordinate Co(II)-based field-induced SIM with negative magnetic anisotropy. The magnetic anisotropy of **1** and **2** and those model complexes with different twist angles have been theoretically studied. The better choice for the larger and negative anisotropy for six-coordinate Co(II) is those of trigonal prismatic geometry, which is consistent with those reported experimental and theoretical works.¹² But our calculations predict that Ni(II) complex with trigonal antiprism would exhibit large easy-axis anisotropy.

Conflicts of interest

There are no conflicts to declare.

Acknowledgements

We are grateful for the financial support from the Natural Science Grant of China (No. 21471078 to XTC, and 11774178 to YQZ), and the US National Science Foundation (CHE-1633870 to ZLX). The National High Magnetic Field Laboratory is funded by the National Science Foundation via Cooperative Agreement No. DMR-1157490 and the State of Florida.

Notes and references

- 1 (a) D. Gatteschi and R. Sessoli, *Angew. Chem., Int. Ed.*, 2003, **42**, 268; (b) W. Wernsdorfer and R. Sessoli, *Science*, 1999, **284**, 133; (c) M. N. Leuenberger and D. Loss, *Nature*, 2001, **410**, 789; (d) R. E. P. Winpenny, *Angew. Chem., Int. Ed.*, 2008, **47**, 7992; (e) D. Gatteschi, R. Sessoli and J. Villain, *Molecular Nanomagnets*, Oxford University Press, Oxford, UK, 2006.
- 2 (a) R. Sessoli, H. L. Tsai, A. R. Schake, S. Wang, J. B. Vincent, K. Folting, D. Gatteschi, G. Christou and D. N. Hendrickson, *J. Am. Chem. Soc.*, 1993, **115**, 1804; (b) R. Sessoli, D. Gatteschi, A. Caneschi and M. A. Novak, *Nature*, 1993, **365**, 141; (c) R. Bagai and G. Christou, *Chem. Soc. Rev.*, 2009, **38**, 1011; (d) D. Gatteschi, R. Sessoli and A. Cornia, *Chem. Commun.*, 2000, 725; (e) K. S. Pedersen, J. Bendix and R. Clérac, *Chem. Commun.*, 2014, **50**, 4396; (f) M. Murrie, *Chem. Soc. Rev.*, 2010, **39**, 1986.
- 3 (a) D. N. Woodruff, R. E. P. Winpenny and R. A. Layfield, *Chem. Rev.*, 2013, **113**, 5110; (b) H. L. C. Feltham and S. Brooker, *Coord. Chem. Rev.*, 2014, **276**, 1.
- 4 N. Magnani and R. Caciuffo, *Inorganics*, 2018, **6**, 26.
- 5 (a) G. A. Craig and M. Murrie, *Chem. Soc. Rev.* 2015, **44**, 2135; (b) A. K. Bar, C. Pichon and J.-P. Sutter, *Coord. Chem. Rev.*, 2016, **308**, 346; (c) J. M. Frost, K. L. M. Harriman and M. Murugesu, *Chem. Sci.*, 2016, **7**, 2470; (d) M. Atanasov, D. Aravena, E. Sutura, E. Bill, D. Maganas and F. Neese, *Coord. Chem. Rev.*, 2015, **289–290**, 177; (e) S. Gómez-Coca, D. Aravena, R. Morales and E. Ruiz, *Coord. Chem. Rev.*, 2015, **289–290**, 379.

- 6 D. E. Freedman, W. H. Harman, T. D. Harris, G. J. Long, C. J. Chang and J. R. Long, *J. Am. Chem. Soc.*, 2010, **132**, 1224.
- 7 M. Atzori, L. Tesi, E. Morra, M. Chiesa, L. Sorace and R. Sessoli, *J. Am. Chem. Soc.*, 2016, **138**, 2154.
- 8 (a) J. Vallejo, A. Pascual-Álvarez, J. Cano, I. Castro, M. Julve, F. Lloret, J. Krzystek, G. D. Munno, D. Armentano, W. Wernsdorfer, R. Ruiz-García and E. Pardo, *Angew. Chem. Int. Ed.*, 2013, **52**, 14075; (b) M. Ding, G. E. Cutsail III, D. Aravena, M. Amoza, M. Rouzières, P. Dechambenoit, Y. Losovyj, M. Pink, E. Ruiz, R. Clérac and J. M. Smith, *Chem. Sci.*, 2016, **7**, 6132.
- 9 (a) J. M. Zadrozny, D. J. Xiao, M. Atanasov, G. J. Long, F. Grandjean, F. Neese and J. R. Long, *Nat. Chem.*, 2013, **5**, 577; (b) M. Atanasov, J. M. Zadrozny, J. R. Long and F. Neese, *Chem. Sci.*, 2013, **4**, 139; (c) A. K. Bar, C. Pichon, N. Gogoi, C. Duhayon, S. Ramasesha and J.-P. Sutter, *Chem. Commun.*, 2015, **51**, 3616; (d) S. Mossin, B. L. Tran, D. Adhikari, M. Pink, F. W. Heinemann, J. Sutter, R. K. Szilagy, K. Meyer and D. J. Mindiola, *J. Am. Chem. Soc.*, 2012, **134**, 13651.
- 10 (a) Y.-S. Meng, Z. Mo, B.-W. Wang, Y.-Q. Zhang, L. Deng and S. Gao, *Chem. Sci.*, 2015, **6**, 7156; (b) X.-N. Yao, J.-Z. Du, Y.-Q. Zhang, X.-B. Leng, M.-W. Yang, S.-D. Jiang, Z.-X. Wang, Z.-W. Ouyang, L. Deng, B.-W. Wang and S. Gao, *J. Am. Chem. Soc.*, 2017, **139**, 373; (c) A. Eichhöfer, Y. Lan, V. Mereacre, T. Bodenstein and F. Weigend, *Inorg. Chem.*, 2014, **53**, 1962; (d) S. Gomez-Coca, E. Cremades, N. Aliaga-Alcalde and E. Ruiz, *J. Am. Chem. Soc.*, 2013, **135**, 7010; (e) F. Habib, O. R. Luca, V. Vieru, M. Shiddiq, I. Korobkov, S. I. Gorelsky, M. K. Takase, L. F.

- Chibotaru, S. Hill, R. H. Crabtree and M. Murugesu, *Angew. Chem., Int. Ed.*, 2013, **52**, 11290; (f) D. Schweinfurth, M. G. Sommer, M. Atanasov, S. Demeshko, S. Hohloch, F. Meyer, F. Neese and B. Sarkar, *J. Am. Chem. Soc.*, 2015, **137**, 1993; (g) P. Antal, B. Drahoš, R. Herchel and Z. Trávníček, *Inorg. Chem.* 2016, **55**, 5957; (h) L. Chen, H.-H. Cui, S. E. Stavretis, S. C. Hunter, Y.-Q. Zhang, X.-T. Chen, Y.-C. Sun, Z. Wang, Y. Song, A. A. Podlesnyak, Z.-W. Ouyang and Z.-L. Xue, *Inorg. Chem.*, 2016, **55**, 12603; (i) L. Chen, J. Wang, J.-M. Wei, W. Wernsdorfer, X.-T. Chen, Y.-Q. Zhang, Y. Song and Z.-L. Xue, *J. Am. Chem. Soc.*, 2014, **136**, 12213.
- 11 (a) J. Vallejo, I. Castro, R. Ruiz-García, J. Cano, M. Julve, F. Lloret, G. De Munno, W. Wernsdorfer and E. Pardo, *J. Am. Chem. Soc.*, 2012, **134**, 15704; (b) E. Colacio, J. Ruiz, E. Ruiz, E. Cremades, J. Krzystek, S. Carretta, J. Cano, T. Guidi, W. Wernsdorfer and E. K. Brechin, *Angew. Chem., Int. Ed.* 2013, **52**, 9130; (c) S. Gómez-Coca, A. Urtizberea, E. Cremades, P. J. Alonso, A. Camón, E. Ruiz and F. Luis, *Nat. Commun.*, 2014, **5**, 4300; (d) R. Herchel, L. Váhovská, I. Potočňák and Z. Trávníček, *Inorg. Chem.*, 2014, **53**, 5896; (e) R. Díaz-Torres, M. Menelaou, O. Roubeau, A. Sorrenti, G. Brandariz-de-Pedro, E. C. Sañudo, S. J. Teat, J. Fraxedas, E. Ruiz and N. Aliaga-Alcalde, *Chem. Sci.*, 2016, **7**, 2793; (f) A. V. Paliy, D. V. Korchagin, E. A. Yureva, A. V. Akimov, E. Y. Misochko, G. V. Shilov, A. D. Talantsev, R. B. Morgunov, S. M. Aldoshin and B. S. Tsukerblat, *Inorg. Chem.*, 2016, **55**, 9696; (g) D. V. Korchagin, A. V. Paliy, E. A. Yureva, A. V. Akimov, E. Y. Misochko, G. V. Shilov, A. D. Talantsev, R. B. Morgunov, A.

- A. Shakin, S. M. Aldoshin and B. S. Tsukerblat, *Dalton Trans.*, 2017, **46**, 7540;
- (h) A. Świtlicka-Olszewska, J. Palion-Gazda, T. Klemens, B. Machura, J. Vallejo, J. Cano, F. Lloret and M. Julve, *Dalton Trans.*, 2016, **45**, 10181; (i) J. P. S. Walsh, G. Bowling, A.-M. Ariciu, N. F. M. Jailani, N. F. Chilton, P. G. Waddell, D. Collison, F. Tuna and L. J. Higham, *Magnetochem.*, 2016, **2**, 23; (j) L. Chen, J. Zhou, H.-H. Cui, A.-H. Yuan, Z. Wang, Y.-Q. Zhang, Z.-W. Ouyang and Y. Song, *Dalton Trans.*, 2018, **47**, 2506; (k) E. A. Buvaylo, V. N. Kokozay, O. Y. Vassilyeva, B. W. Skelton, A. Ozarowski, J. Titiš, B. Vranovičová and R. Boča, *Inorg. Chem.*, 2017, **56**, 6999. (l) J. Li, Y. Han, F. Cao, R.-M. Wei, Y.-Q. Zhang and Y. Song, *Dalton Trans.*, 2016, **45**, 9279; (m) Y.-Z. Zhang, S. Gómez-Coca, A. J. Brown, M. R. Saber, X. Zhang and K. R. Dunbar, *Chem. Sci.*, 2016, **7**, 6519; (n) J. Zhang, J. Li, C. Yuan, Y.-Q. Zhang and Y. Song, *Inorg. Chem.*, 2018, **57**, 3803;
- 12 (a) Y.-Y. Zhu, C. Cui, Y.-Q. Zhang, J.-H. Jia, X. Guo, C. Gao, K. Qian, S.-D. Jiang, B.-W. Wang, Z.-M. Wang and S. Gao, *Chem. Sci.*, 2013, **4**, 1802; (b) Y.-Y. Zhu, Y.-Q. Zhang, T.-T. Yin, C. Gao, B.-W. Wang and S. Gao, *Inorg. Chem.*, 2015, **54**, 5475; (c) V. V. Novikov, A. A. Pavlov, Y. V. Nelyubina, M.-E. Boulon, O. A. Varzatskii, Y. Z. Voloshin and R. E. P. Winpenny, *J. Am. Chem. Soc.*, 2015, **137**, 9792; (d) A. A. Pavlov, Y. V. Nelyubina, S. V. Kats, L. V. Penkova, N. N. Efimov, A. O. Dmitrienko, A. V. Vologzhanina, A. S. Belov, Y. Z. Voloshin and V. V. Novikov, *J. Phys. Chem. Lett.*, 2016, **7**, 4111; (e) T. J. Ozumerzifon, I. Bhowmick, W. C. Spaller, A. K. Rappe and M. P. Shores, *Chem. Commun.*, 2017,

- 53**, 4211; (f) Y. Peng, T. Bodenstein, K. Fink, V. Mereacre, C. E. Ansona and A. K. Powell, *Phys. Chem. Chem. Phys.*, 2016, **18**, 30135; (g) S. Gomez-Coca, E. Cremades, N. Aliaga-Alcalde and E. Ruiz, *J. Am. Chem. Soc.*, 2013, **135**, 7010.
- 13 (a) W. Lin, T. Bodenstein, V. Mereacre, K. Fink and A. Eichhöfer, *Inorg. Chem.*, 2016, **55**, 2091; (b) J. Miklovič, D. Valigura, R. Boča and J. Titiš, *Dalton Trans.*, 2015, **44**, 12484; (c) D. Lomjanský, J. Moncol', C. Rajnák, J. Titiš and R. Boča, *Chem. Commun.*, 2017, **53**, 6930; (d) K. E. R. Marriott, L. Bhaskaran, C. Wilson, M. Medarde, S. T. Ochsenbein, S. Hill and M. Murrie, *Chem. Sci.*, 2015, **6**, 6823.
- 14 R. Boča, C. Rajnák, J. Titiš and D. Valigura, *Inorg. Chem.*, 2017, **56**, 1478.
- 15 (a) Y.-F. Deng, T. Han, Z. Wang, Z. Ouyang, B. Yin, Z. Zheng, J. Krzystek and Y.-Z. Zheng, *Chem. Commun.*, 2015, **51**, 17688; (b) A. Cornia, L. Rigamonti, S. Boccedi, R. Clérac, M. Rouzières and L. Sorace, *Chem. Commun.*, 2014, **50**, 15191.
- 16 (a) J. Martínez-Lillo, T. F. Mastropietro, E. Lhotel, C. Paulsen, J. Cano, G. D. Munno, J. Faus, F. Lloret, M. Julve, S. Nellutla and J. Krzystek, *J. Am. Chem. Soc.*, 2013, **135**, 13737; (b) K. S. Pedersen, M. Sigrist, M. A. Sørensen, A.-L. Barra, T. Weyhermiiller, S. Piligkos, C. A. Thuesen, M. G. Vinum, H. Mutka, H. Weihe, R. Clérac and J. Bendix, *Angew. Chem. Int. Ed.*, 2014, **53**, 1351.
- 17 (a) S.-D. Jiang, D. Maganas, N. Levesanos, E. Ferentinos, S. Haas, K. Thirunavukkuarasu, J. Krzystek, M. Dressel, L. Bogani, F. Neese and P. Kyritsis, *J. Am. Chem. Soc.*, 2015, **137**, 12923; (b) S. Gómez-Coca, E. Cremades, N. Aliaga-Alcalde and E. Ruiz, *Inorg. Chem.*, 2014, **53**, 676; (c) R. Ruamps, R.

- Maurice, L. Batchelor, M. Boggio-Pasqua, R. Guillot, A. L. Barra, J. Liu, E.-E. Bendeif, S. Pillet, S. Hill, T. Mallah and N. Guihéry, *J. Am. Chem. Soc.*, 2013, **135**, 3017; (d) R. Ruamps, L. J. Batchelor, R. Maurice, N. Gogoi, P. Jiménez-Lozano, N. Guihéry, C. de Graaf, A.-L. Barra, J.-P. Sutter and T. Mallah, *Chem. Eur. J.*, 2013, **19**, 950; (e) I. Nemeč, R. Herchel, I. Svoboda, R. Boča and Z. Trávníček, *Dalton Trans.*, 2015, **44**, 9551.
- 18 (a) J. Krzystek, S. A. Zvyagin, A. Ozarowski, S. Trofimenko and J. Telser, *J. Magn. Reson.*, 2006, **178**, 174; (b) J. Krzystek, J.-H. Park, M. W. Meisel, M. A. Hitchman, H. Stratemeier, L.-C. Brunel and J. Telser, *Inorg. Chem.*, 2002, **41**, 4478; (c) P. J. Desrochers, J. Telser, S. A. Zvyagin, A. Ozarowski, J. Krzystek and D. A. Vicic, *Inorg. Chem.*, 2006, **45**, 8930; (d) I. Nieto, R. P. Bontchev, A. Ozarowski, D. Smirnov, J. Krzystek, J. Telser, J. M. Smith, *Inorg. Chim. Acta*, 2009, **362**, 4449; (e) J.-N. Rebilly, G. Charron, E. Rivière, R. Guillot, A.-L. Barra, M. D. Serrano, J. van Slageren and T. Mallah, *Chem. Eur. J.*, 2008, **14**, 1169; (f) B. Cahier, M. Perfetti, G. Zakhia, D. Naoufal, F. El-Khatib, R. Guillot, E. Rivière, R. Sessoli, A.-L. Barra, N. Guihéry and T. Mallah, *Chem. Eur. J.*, 2017, **23**, 3648.
- 19 (a) J. Krzystek, A. Ozarowski and J. Telser, *Coord. Chem. Rev.*, 2006, **250**, 2308; (b) G. Rogez, J.-N. Rebilly, A.-L. Barra, L. Sorace, G. Blondin, N. Kirchner, M. Duran, J. van Slageren, S. Parsons, L. Ricard, A. Marvilliers and T. Mallah, *Angew. Chem. Int. Ed.*, 2005, **44**, 1876; (c) D. Dobrzyńska, L. B. Jerzykiewicz, M. Duczmal, A. Wojciechowska, K. Jabłońska, J. Palus and A. Ozarowski, *Inorg.*

- Chem.*, 2006, **45**, 10479; (d) G. Charron, F. Bellot, F. Cisnetti, G. Pelosi, J.-N. Rebilly, E. Rivère, A.-L. Barra, T. Mallah and C. Policar, *Chem. Eur. J.*, 2007, **13**, 2774; (e) A. Wojciechowska, M. Daszkiewicz, Z. Staszak, A. Trusz-Zdybek, A. Bieńko and A. Ozarowski, *Inorg. Chem.*, 2011, **50**, 11532; (f) D. Maganas, J. Krzystek, E. Ferentinos, A. M. Whyte, N. Robertson, V. Psycharis, A. Terzis, F. Neese and P. Kyritsis, *Inorg. Chem.*, 2012, **51**, 7218; (g) D. Schweinfurth, J. Krzystek, I. Schapiro, S. Demeshko, J. Klein, J. Telsler, A. Ozarowski, C.-Y. Su, F. Meyer, M. Atanasov, F. Neese and B. Sarkar, *Inorg. Chem.*, 2013, **52**, 6880; (h) A. Wojciechowska, J. Janczak, Z. Staszak, M. Duczmal, W. Zierkiewicz, J. Tokar and A. Ozarowski, *New J. Chem.*, 2015, **39**, 6813; (i) G. Charron, E. Malkin, G. Rogez, L. J. Batchelor, S. Mazerat, R. Guillot, N. Guihéry, A.-L. Barra, T. Mallah and H. Bolvin, *Chem. Eur. J.*, 2016, **22**, 16850.
- 20 (a) E. Fursova, G. Romanenko, R. Sagdeev and V. Ovcharenko, *Polyhedron*, 2014, **81**, 27; (b) E. Fursova, G. Romanenko and V. Ovcharenko, *Polyhedron*, 2013, **62**, 274.
- 21 (a) B. Cage, A. Hassan, L. Pardi, J. Krzystek, L.C. Brunel and N.S. Dalal, *J. Mag. Reson.*, 1997, **124**, 495; (b) A. Hassan, L. Pardi, J. Krzystek, A. Sienkiewicz, P. Goy, M. Rohrer and L.C. Brunel, *J. Mag. Reson.*, 2000, **142**, 300.
- 22 (a) M. Llunell, D. Casanova, J. Cirera, P. Alemany and S. Alvarez, *Shape Program*, Version 2.1, 2013; (b) S. Alvarez, P. Alemany, D. Casanova, J. Cirera, M. Llunell and D. Avnir, *Coord. Chem. Rev.*, 2005, **249**, 1693.
- 23 (a) F. Lloret, M. Julve, J. Cano, R. Ruiz-García and E. Pardo, *Inorg. Chim. Acta*,

- 2008, 361, 3432; (b) J. Titiš and R. Boča, *Inorg. Chem.*, 2011, **50**, 11838.
- 24 (a) Simulations were performed using SPIN developed by Andrew Ozarowski in National High Magnetic Field Laboratory, US; (b) F. R. Xavier, A. Neves, A. Casellato, R. A. Peralta, A. J. Bortoluzzi, B. Szpoganicz, P. C. Severino, H. Terenzi, Z. Tomkowicz, S. Ostrovsky, W. Haase, A. Ozarowski, J. Krzystek, J. Telsler, G. Schenk and L. R. Gahan, *Inorg. Chem.*, 2009, **48**, 7905.
- 25 (a) N. F. Chilton, R. P. Anderson, L. D. Turner, A. Soncini and K. S. Murray, *J. Comput. Chem.*, 2013, **34**, 1164; (b) N. F. Chilton, *PHI User Manual v3*, 2018.
- 26 L. Ungur and L. F. Chibotaru. *Chem. Eur. J.*, 2017, **23**, 3708.
- 27 G. Karlström, R. Lindh, P. -Å. Malmqvist, B. O. Roos, U. Ryde, V. Veryazov, P. -O. Widmark, M. Cossi, B. Schimmelpfennig, P. Neogrady and L. Seijo, *Comput. Mater. Sci.*, 2003, **28**, 222.
- 28 F. E. Mabbs and D. Collison, *Electron Paramagnetic Resonance of Transition Metal Compounds*, Elsevier, Amsterdam, 1992.
- 29 J. Krzystek and J. Telsler, *Dalton Trans.*, 2016, **45**, 16751.
- 30 (a) Y.-N. Guo, G.-F. Xu, Y. Guo and J. Tang, *Dalton Trans.*, 2011, **40**, 9953; (b) K. S. Cole and R. H. Cole, *J. Chem. Phys.*, 1941, **9**, 341.
- 31 (a) R. L. Carlin and A. J. van Duyneveldt, *Magnetic Properties of Transition Metal compounds*, Springer-Verlag, New York, 1976; (b) K.N. Shrivastava, *Phys. Status Solidi B*, 1983, **117**, 437.
- 32 L. Ungur and L. F. Chibotaru, *Inorg. Chem.*, 2016, **55**, 10043.

Magnetic anisotropy and relaxation behavior of six-coordinate tris(pivalato)-Co(II) and -Ni(II) complexes

Shu-Yang Chen, Hui-Hui Cui, Yi-Quan Zhang, Zhenxing Wang, Zhong-Wen Ouyang,

Lei Chen, Xue-Tai Chen, Hong Yan, Zi-Ling Xue

Magnetic measurements, HF-EPR and theoretical calculations have been used to study the magnetic anisotropy of six-coordinate field-induced single ion magnet (NBu₄)[Co(piv)₃] and its Ni analogue.

